Thin Solid Films 702 (2020) 137982

Contents lists available at ScienceDirect

Thin Solid Films

journal homepage: www.elsevier.com/locate/tsf

Selective etching of nanostructured a-Si:Al and its effect on porosity, Al gradient and surface oxidation

T. Kjeldstad[a,*], A. Thøgersen[b], M. Stange[b], I.T. Jensen[b], O. Nilsen[c], A. Galeckas[a], E. Monakhov[a]

[a] Department of Physics/Centre for Materials Science and Nanotechnology, University of Oslo, P.O. Box 1048 Blindern, Oslo, N-0316, Norway
[b] SINTEF Materials Physics, P.O. Box 124 Blindern, Oslo, 0314, Norway
[c] Department of Chemistry/Centre for Materials Science and Nanotechnology, University of Oslo, P.O. Box 1033 Blindern, Oslo, N-0316, Norway

ARTICLE INFO

Keywords:
Amorphous silicon
Self-assembly
Aluminum
Nanowires
Nanoporous
Selective etching

ABSTRACT

Nanoporous amorphous silicon (a-Si) with <5 nm cylindrical pores have been fabricated by phase separation of aluminum (Al) and silicon, forming self-assembled Al nanowires (NWs), followed by subsequent removal of Al by wet etching. This work studies the removal process of the Al NWs when using the different etchants HCl, H_3PO_4, and H_2SO_4. Total reflectance measurements are used in combination with theoretical modeling to estimate the lateral gradient of Al concentration formed during the etching process. X-ray Photoelectron Spectroscopy is used to show that the choice of Al etching agent has implications for the surface states of the remaining a-Si matrix. We have found that H_3PO_4 is the most efficient etching agent, while HCl provides a less oxidized a-Si matrix in addition to the least reflective surface. By varying the etching agent, the degree of surface oxidation and shape of Al gradient throughout the film can be tuned.

1. Introduction

Nanostructured silicon (Si) such as porous silicon and Si nanoholes has received a lot of attention because of its potential in photovoltaics, battery technology and as a host material for particles, molecules, and metals [1–8]. Porous Si is normally fabricated through anodization of crystalline Si, and may be manufactured with a variety of pore sizes. The porous Si with pore sizes in the nanometer range has a more sponge-like structure, rather than the cylindrical pores that are found in, for example, anodic alumina [9]. Therefore, structures such as anodic alumina are often preferred as a template for deposition of arrays of nanowires (NWs) or nanotubes [10–12]. Anodic alumina may be fabricated with diameters down to approximately 10 nm, excluding it as a template for smaller structures often necessary for the exploitation of quantum confinement or other size-dependent effects [13–15].

A combination of cylindrical shape pores of merely a few nanometer diameters and the advantageous properties of Si can be achieved in a nanostructured thin film manufactured by sputtering of aluminum (Al) and Si [16–18]. This method utilizes the immiscibility of Al and Si, where Al self-assembles as nanowires inside an a-Si matrix given the correct aspect ratio of sputtered Al and Si, resulting in a nanostructured a-Si:Al film. We have previously shown that by co-sputtering Al and Si at room temperature, vertically aligned 5 nm diameter Al NWs can be formed and that subsequent removal of the Al NWs gives a nanoporous film of a-Si with an interpore distance of approximately 5 nm [18,19].

As removal of the Al NWs from the nanostructured a-Si:Al is a prerequisite for many of the potential applications, process control and insight into the implications that the removal process has on the remaining a-Si is paramount. Wet etching is a simple, inexpensive and easily scalable technique that suits perfectly this task. In our previous work, we have used an aqueous solution of HCl to selectively remove the Al NWs and established that the removal process may be monitored on a macroscopic scale by measuring the reflectance of the film [19,20]. HCl is not the only potential etching agent and previous works by others have used concentrated H_2SO_4 and H_3PO_4 to selectively remove Al, but no details have been given on the impact of the etching process on the remaining a-Si[16,17].

In this work, we continue our investigations of Al NW removal by investigating the effects of using the etching agents H_2SO_4 and H_3PO_4, in addition to HCl. The surface states of the nanoporous a-Si is characterized by X-ray photoelectron spectroscopy (XPS) and porosity is measured by ellipsometric porosimetry (EP). We continue our work on utilizing UV–vis spectroscopy as a method to monitor the Al NW removal, by modeling the reflectance using the transfer matrix model as a method of estimating the Al content as a function of depth during the etching process [19,20]. The results from the model are supported by EP and energy dispersive spectroscopy (EDS) measurements using Transmission Electron Microscopy (TEM).

* Corresponding author.
E-mail address: torunn.kjeldstad@fys.uio.no (T. Kjeldstad).

https://doi.org/10.1016/j.tsf.2020.137982
Received 4 November 2019; Received in revised form 7 March 2020; Accepted 25 March 2020
Available online 05 April 2020

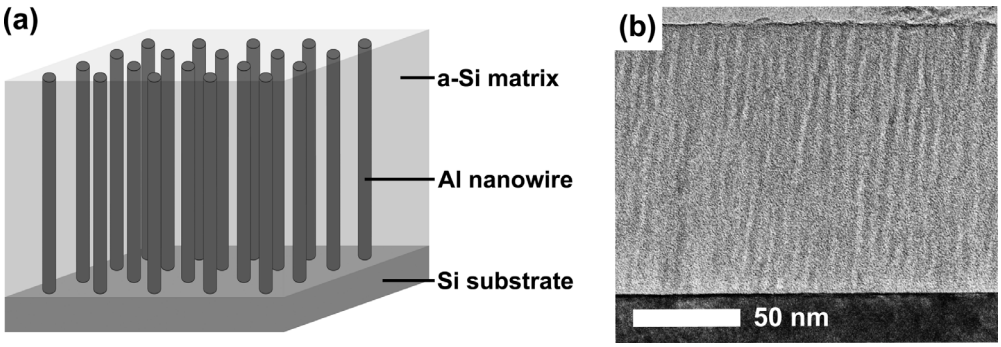

Fig. 1. (a) Schematic illustration of the nanostructures a-Si:Al and (b) cross-section TEM image of nanoporous a-Si.

2. Methods

The nanostructured a-Si:Al was produced by co-sputtering of Si and Al with a CVC 601 magnetron sputtering system onto single-crystalline (100) substrates. The system consisted of two 8″ targets with normal sputter angle and 6 cm distance between substrate and targets. The deposition was performed at room temperature with thin alternating layers with a ratio of approximately 40 at.% Al and 60 at.% Si obtained by using a power of 400 W for Si and 150 W for Al with a substrate rotation of 2.5 rpm and a sputtering time of 22 min, resulting in a 100 nm thick film. For a more detailed description of the deposition process see work by Thøgersen et al. [18].. The sputtering process was carried out in an argon atmosphere at 0.4 Pa and with a hydrogen flow of 4 ml/min. The formation of Al nanowires was confirmed by TEM. Fig. 1(a) shows a schematic illustration of the nanostructure and Fig. 1(b) shows a cross section TEM image of the nanostructures a-Si:Al where the Al NWs have been removed . For TEM images with corresponding EDS line scan of the nanostructured a-Si:Al, both as-grown and with Al NWs removed, please see Ref. [19].

Al NWs were removed by a wet etch process in a 1:1 solution of 37% HCl, 1:1 solution of 85% H_3PO_4, 1:1 and 1:50 solution of 95% H_2SO_4 diluted in deionized water. The etching process was done at room temperature without agitation of the solution. After etching, the samples were rinsed in deionized water.

The surface states of Si and Al were measured by XPS in a KRATOS AXIS ULTRA^{DLD} instrument using monochromatic Al Kα radiation ($h\nu$ = 1486.6 eV). The X-ray source was operated at 10 mA and 15 kV, and high-resolution spectra were acquired with a step size of 0.1 eV and pass energy of 40 eV. The spectra were fitted with the computer program CasaXPS Version 2.3.17PR1.1. The spectra were referenced to the native Si peak and fitted to known values of the different oxidation states of Si. For elemental Si, two spin-orbit coupled peaks were fitted with asymmetrical peaks with a tail length of 1.5, tail scale of 0.6% and 70% Gaussian (GL(30)T(1.5)). The Si-2p spin-orbit coupled peaks were fitted with a set peak shift of 0.6 eV, the same full width half maximum (FWHM) for both spin orbit coupled peaks, and an area constraint ratio between 2p-3/2/2p-½ of 2. However, small variations have been considered from these optimum values. To fit the remaining part, four Gaussian peaks were used and peak position were adjusted according to known values of the different oxidation states [21–24]. In the fitting, the Full Width Half Maximum (FWHM) was limited to 1.5.

Optical characterization was performed by measuring total reflectance at room temperature using a Shimadzu SolidSpec-3700/3700DUV spectrophotometer equipped with an integrating sphere and allowing measurements within the wavelength range from 186 nm to 2500 nm.

Cross-sectional TEM imaging and energy dispersive spectroscopy (EDS) was performed using an FEI Titan G2 60-300 microscope with an acceleration voltage of 300 kV equipped with a with a super EDX detector. The cross-sectional samples were prepared by grinding and ion-milling using a Gatan Precision Ion Position System with 4 kV gun voltage.

Porosity was investigated by ellipsometric porosimetry using a J.A. Woollam M-2000 Spectroscopic Ellipsometer with an additional environmental cell. The ellipsometric data were modeled by Cauchy models using the CompleteEASE Software. Pore volume was determined by modeling the water adsorption/desorption isotherm using the Lorenz-Lorenz effective medium model.

3. Results

3.1. Surface oxidation

As the Al NWs are removed and the a-Si is exposed, the latter will begin to interact with the etchant. The degree of interaction, such as oxidation of the a-Si, can impact the properties of the remaining a-Si through spatial confinement of the a-Si [25,26]. To evaluate the effect the etchant has on the a-Si, XPS was performed. XPS is a surface-sensitive technique, it is therefore expected that information is provided from the first 10 nm of the a-Si:Al nanostructure. 5 h of etching was considered sufficient for Al removal in this top layer. Fig. 2 shows the XPS spectra of the Si-2p peak for samples etched for 5 h in HCl, concentrated H_2SO_4 and H_3PO_4. The Si-2p peak shows peaks from both the a-Si matrix as well as oxidized Si. To quantify the composition, the spectra were fitted as described under Methods. Peak positions and the corresponding FWHM parameters for the peaks which correspond to Si (Si^0), Si_2O (Si^+), SiO (Si^{2+}), Si_2O_3 (Si^{3+}) and SiO_2 (Si^{4+}) are given in

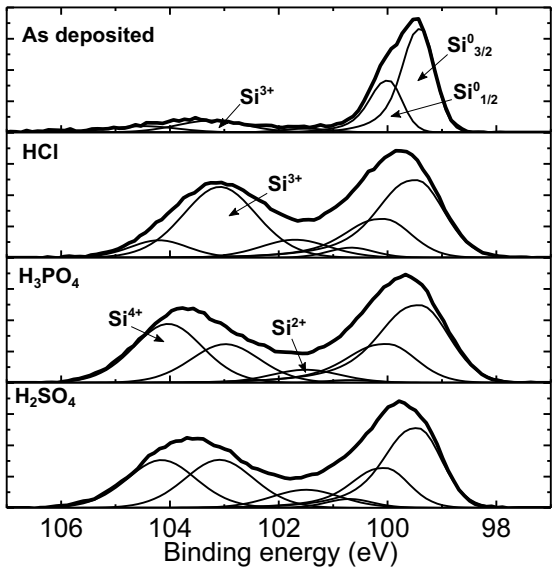

Fig. 2. XPS spectra of Si-2p peak for an as deposited film and samples etched for 5 h in HCl, H_3PO_4 and concentrated H_2SO_4, respectively. Gaussian peaks fitted to the spectra for quantification of Si oxidation state.

Table 1
The binding energy (EB), full with half maximum (FWHM) and atomic% for different oxidation states of Si present in etched a-Si:Al.

Oxidation state	EB [eV] ± 0.1 eV	FWHM [eV]	Atomic% of Si		
			HCl	H_3PO_4	Conc. H_2SO_4
Si^0	99.4, 100.04	1.0–1.2	51	53	47
Si^+	100.7	1	3	1	3
Si^{2+}	101.5	1.5	8	5	8
Si^{3+}	103.9	1.5	32	16	21
Si^{4+}	104.1	1.3–1.15	6	25	21

Table 1. This analysis shows that etching in concentrated H_2SO_4 and H_3PO_4 results in a larger fraction of Si^{4+} as compared to HCl, which consists of mostly Si^{3+}. In addition, the remaining elemental Si after etching is close to 50%, and is comparable for all three etching processes. It may be noted that 5 h etching in H_2SO_4 is not sufficient to remove Al in the top layer of the film, thus the fraction of elemental Si may be somewhat higher than for a fully etched sample, as the areas where NWs still remain will not have been exposed to the etchant resulting in a larger amount of elemental Si.

3.2. Reflectance and its dependence on the Al etching process

As XPS only gives information on the top surface of the nanoporous a-Si, other techniques were used to obtain information about the whole 100 nm nanostructured film. We have previously shown that measurement of total reflectance is a simple way of monitoring the etching process [19]. To investigate the development of reflectance during Al NW removal, etching and measurement of total reflectance were alternated for samples etched in HCl, H_3PO_4, and H_2SO_4. To avoid unnecessary exposure of the nanoporous a-Si matrix, the etching process was stopped when the characteristic shape of an interference peak for a ~100 nm film with a refractive index of ~1.55 appeared. This peak is observed in the wavelength range between 400 and 500 nm, with a full width half maximum of approximately 200 nm. As previously shown, this indicates that a large amount of Al has been removed from the thin film [19]. The solid lines in Fig. 3 (a–c) show the measured total reflectance for samples etched in HCl, H_3PO_4, and H_2SO_4 for different etching times. The dotted lines in Fig. 3 (a–c) and the Al content as a function of depth shown in Fig. 3 (d–f) is a result of modeling of the reflectance described in the next paragraph. The reflectance shown in Fig. 3 (a–c) is gradually reduced with increasing etching time until the interference peak starts to appear. As shown in Ref [19], the as deposited film has a reflectance of approximately 40–50%, which is reduced by all etchants. However, it takes 2 h of etching to achieve a reflectance of 20% for HCl and H_3PO_4, while 6 h of etching is required for the concentrated H_2SO_4 solution. While the etching process was stopped after 10.5 h and 18 h for H_3PO_4 and HCl, respectively, the interference peak was not clearly visible for concentrated H_2SO_4 even after 27 h when the experiment was stopped.

The change in reflectance during the etching process is a result of Al gradually being removed, causing a change in the Al concentration as a function of depth. As the Al NWs and interpore distance is much smaller than the wavelength of light, the nanostructured film may be considered optically homogenous [27]. Therefore, this depth-dependent Al concentration may be estimated by simulating the reflectance using the transfer matrix model (TMM) and approximating the nanostructure to consist of several planar layers with different Al concentrations [28]. For each layer, the effective refractive index is given by mixing the different constituents, a-Si, SiO_2, Al, and air. Several models may be used for this, such as Lorenz-Lorenz and Maxwell Garnett approach [27]. In this work, we have chosen the Bruggeman Effective Medium Approach which is appropriate for more homogeneous mixtures [27]. Thus, the effective refractive index in each layer has been calculated by

$$0 = \sum f_i \left(\frac{N_i^2 - N_{eff}^2}{N_{eff}^2 + L_j(N_i^2 - N_{eff}^2)} \right), \quad (1)$$

where f_i and n_i is the fraction and refractive index of the respective constituent, n_{eff} is the refractive index of the film and L_j is the depolarization factor. For cylindrical inclusions, L_j is set as 1/2, while for spherical inclusion L_j is set as 1/3 [27,29]. Bearing in mind that the as deposited film is comprised of Al nanowires with an aspect ratio of 20 and the etched film consists of cylindrical pores, it may seem reasonable to use a depolarization factor of 1/2. However, the aspect ratio of the Al nanowire is reduced during Al removal, and it may therefore be more appropriate to use the depolarization factor for spherical inclusions. Because of this, the TMM was calculated for both depolarization factors. L_j for cylindrical inclusions was found to give the best fit with the measured reflectance. In the calculations we used known refractive indexes for the bulk material [30–33]. To estimate the volume fraction of a-Si and SiO_2 as a function of Al, we assume that as the Al is removed, half of the remaining elemental silicon is in the form of silicon oxide, which is in accordance with the results from XPS. Due to the volume expansion when Si is oxidized to SiO_2, we assume that the void is reduced by 50%. This gives volume fractions of $V_{SiO2} = 0.5 - V_{Al}$, $V_{a\text{-}Si} = 0.25 + V_{Al}/2$, $V_{air} = 0.25 - V_{Al}/2$. The volume fraction of Al as a function of depth is estimated by an exponential function:

$$V_{Al} = a + b(1 - e^{-cx}), \quad (2)$$

where *a, b* and *c* are fitting parameters. Fig. 4 shows the volume fraction of the film based on the Al gradient that provided the best fit to the reflectance for porous a-Si etched in H_2PO_4 for 10 h. Fig. 3 shows the modeled reflectance (a–c) and the corresponding Al gradient (d–f) for nanostructured a-Si:Al etched in HCl, H_3PO_4, and H_2SO_4. To verify the simulated Al fractions in Fig. 3d-e as a function of depth, the curves have been compared to EDS line scans from TEM investigations. The EDS line scans of the Al, Si and O concentrations through the thin film from an a-Si:Al film etched for 4 h in HCl is shown in Fig. 4. Both line scans are from different areas in the sample within 1 cm proximity of each other. This shows that Al is present as a gradient and there are local deviations in the Al gradient within the film. As the reflectance is measured from a 0.5 cm^2 area, the Al gradient used for the TMM calculation is considered an average within the film.

Fig. 3 shows that there are some deviations between the measured reflectance and the calculated reflectance. The transfer matrix model does not include plasmonic effects from the Al nanowires, which may give deviations on the plasmonic regime [34]. In addition, as shown in Fig. 4, the Al gradient varies and is not necessarily accurately described by the chosen exponential function. Despite these deviations, this model may be used to explain the difference in reflectance development for the different etching processes. The reflectance results show that H_3PO_4 requires a shorter etching time for Al removal, while etching with HCl results in a film with lower overall reflectance during the etching process. The lower reflectance is a result of a more linear Al gradient as compared to the Al gradient achieved by etching in H_3PO_4. This means that the sample etched by H_3PO_4 has a larger Al concentration towards the surface of the thin film, thereby causing higher reflection as compared to the sample etched by HCl.

As shown in Fig. 3(c) and (f), concentrated H_2SO_4 is not suitable for Al removal as the etching stops while still a large fraction of Al remains in the film. Fig. 5(a) shows measured and modeled reflectance of a-Si:Al etched in HCl and a diluted H_2SO_4 (1:50) solution for 48 h. The Al gradient that provided the best fit is given in Fig. 5(b). Etching in diluted H_2SO_4 results in Al removal, but at a much slower rate as compared to HCl and H_3PO_4. This shows that prolonged etching results in almost complete removal of Al and that the concentration of the H_2SO_4 used is important.

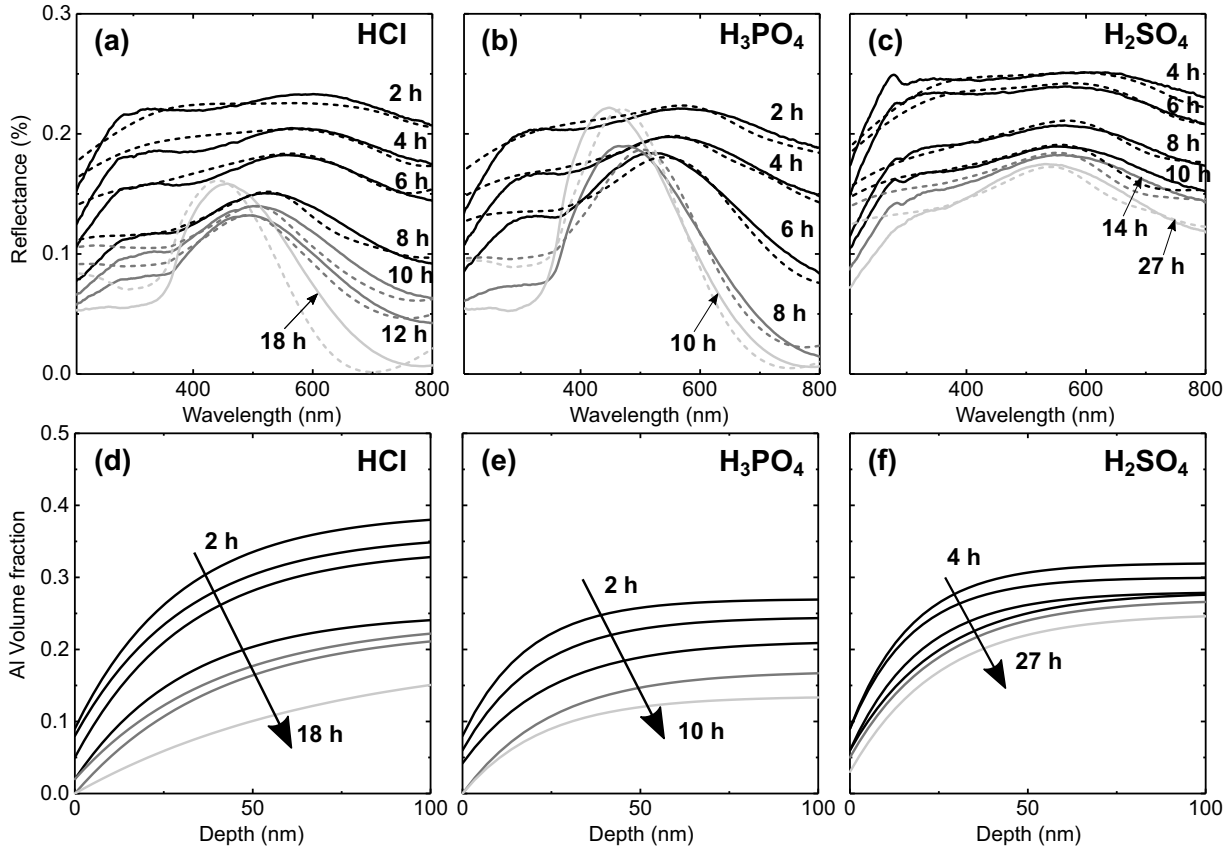

Fig. 3. Reflectance measured for films etched in HCl, H_3PO_4 and H_2SO_4 (solid lines) and the fitted reflectance calculated using the transfer matrix model and Bruggeman Effective Medium Approximation (dotted lines) (a–c). The corresponding Al gradients are plotted on the lower row panels, where the Al volume fraction as a function of depth from film surface for each modeled reflectance is shown in respectively (d–f).

3.3. Porosity

Removal of the Al NWs results in a porous structure consisting of nanoporous a-Si with an oxidized surface, and the estimated volume fraction of air may be deduced from the TMM calculations. To complement the estimated porosity provided by reflectance modeling, ellipsometry porosimetry was performed. Fig. 6 shows the water adsorption within the porous a-Si matrix for the a-Si:Al samples etched in HCl and H_3PO_4 for 18 h and 10.5 h, (a) and (b) respectively, and HCl and diluted H_2SO_4 for 48 h, (c) and (d). The water adsorption is calculated by modeling the measured ellipsometric data in the range from 450 nm to 800 nm during adsorption and desorption with a Cauchy model [35]. The Lorentz-Lorentz effective medium approximation [27] was used to calculate the water content within the pores as a function of vapor pressure based on the change in refractive index. The refractive index was chosen at the wavelength $\lambda = 600$ nm as the Cauchy model gave the best fit at this wavelength. The results show a porosity of 20% for the sample etched in HCl for 18 h and a porosity of 18% for the sample etched in H_3PO_4. These values are comparable with the void fractions calculated using the reflectance data, which give 20% for samples etched in HCl and H_3PO_4. For the sample etched in concentrated H_2SO_4, it was not possible to obtain a sufficient fit of the ellipsometry data to calculate the change in refractive index. This is likely due to the large Al concentration still present in the film.

Fig. 6(c) and (d) shows the hysteresis curve of water adsorption for porous a-Si etched for 48 h in HCl and 1:50 diluted H_2SO_4. The presented results suggest increased etching time increases the porosity to approximately 25%, which is similar to the void fraction estimated from reflectance modeling (23% for sample etched in HCl and 22% for the sample etching in 1:50 H_2SO_4). In addition to increasing the

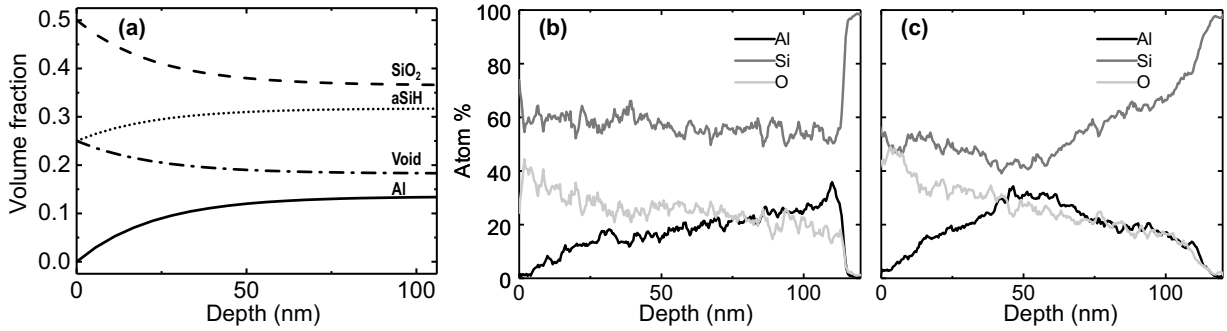

Fig. 4. (a) Volume fraction used to model reflectance for a thin film etched in H_3PO_4 for 10 h. (b) and (c) EDS line scan of cross-section of different areas of a-Si:Al film etched in HCl for 4 h.

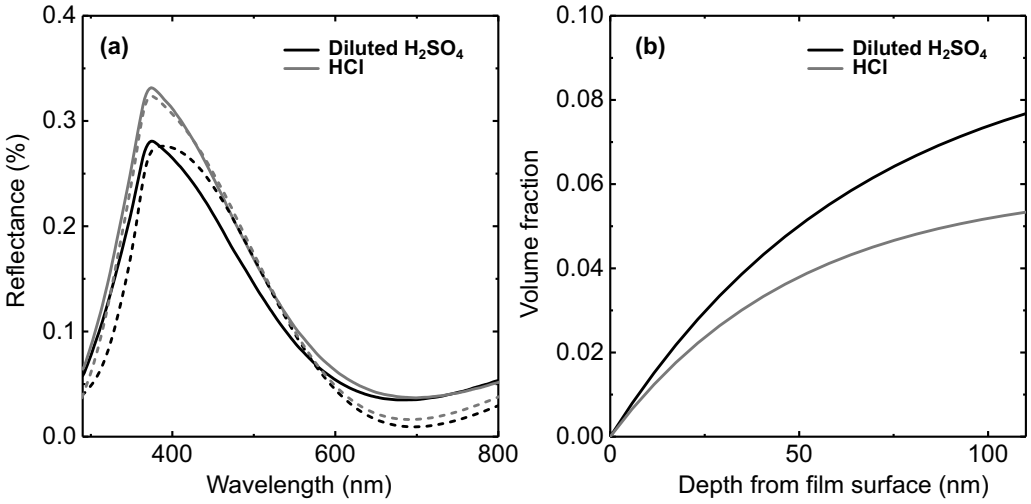

Fig. 5. (a) Measured (solid lines) and simulated (dotted lines) reflectance of porous a-Si etched for 48 h in HCl and diluted H_2SO_4 and the corresponding Al gradient used for the simulation (b).

porosity, the prolonged etching conditions results in a larger hysteresis area, which is typical for inkbottle pores, indicating that the pore diameter at the top of the pore is smaller than the remaining porous cylinder [36]. This effect is larger for the film etched in HCl, which may be explained by longer exposure to the etchant, as HCl etches more efficiently, thus removing the Al earlier and exposing the remaining a-Si for a longer time. Consequently, in case a uniformly porous a-Si is intended for use as a template, it is imperative to optimize the etching time, both to ensure sufficient Al removal and minimize a-Si surface exposure to the etchant.

4. Discussion

Fig. 3 shows that the shapes of Al profiles in the films are different for the three etchants. As care has been taken to ensure that the composition of the three samples is very similar, the differences must be a result of the removal process. Fig. 7 shows time-lapse sequences of the removal of a 200 nm thick Al film deposited by e-beam on Si substrate in the case of HCl and H_3PO_4 treatment. After 7 min of etching, no change can be seen for the sample in H_3PO_4, but in HCl small areas of Al have already been removed. These are assumed to be from defects in the protective oxide layer, enabling HCl to reach the underlying Al, accelerating the removal of Al as flakes, all accompanied by significant evolution of gas. For the sample in H_3PO_4, slow development of bubbles is observed from 7 min and onwards, but no sign of attack of the Al trough defects, such as for the HCl treatment, is observed. This indicates that the Al is evenly etched, probably due to the formation of the low soluble aluminum phosphate on the surface during etching [37].

There are several limiting factors in removal of the Al NWs. Firstly, the naturally occurring oxide on the surface acts as a barrier between Al and the etchant. Secondly, the Al removal is dependent on transport of reaction products from within the pores and availability of etchant at the NW interface. This transport may slow down as the aspect ratio of the pores increase, thus reducing the etching rate. In addition, possible products of the dissolution may act as a limiting factor, as in the case of removal by H_3PO_4, where aluminum phosphate may hinder further

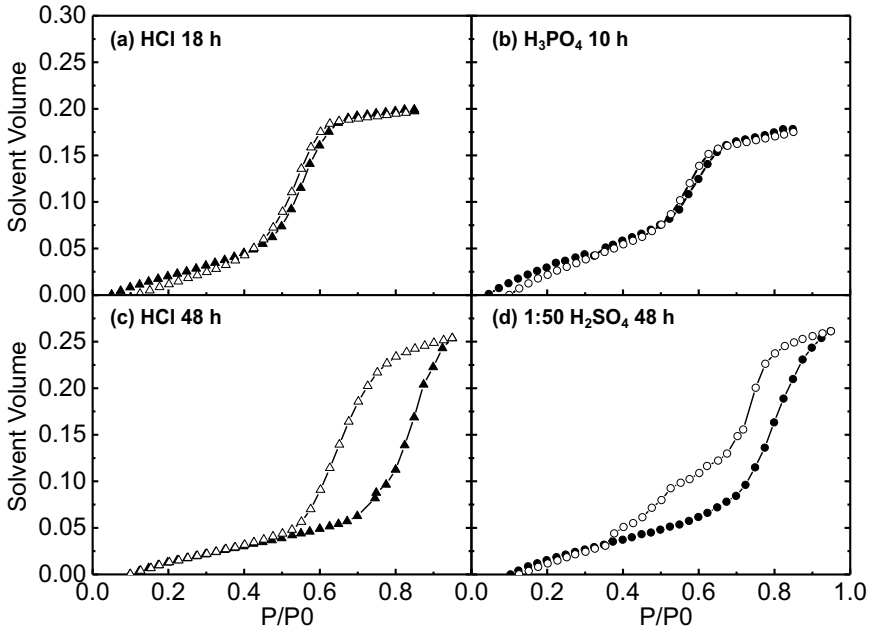

Fig. 6. Solvent volume as a function of partial water pressure during adsorption (solid) and desorption (open) for thin films etched in HCl for 18 h (a) and H_3PO_4 for 10 h (b), and for thin films etched in HCl (c) and diluted H_2SO_4 for 48 h (d).

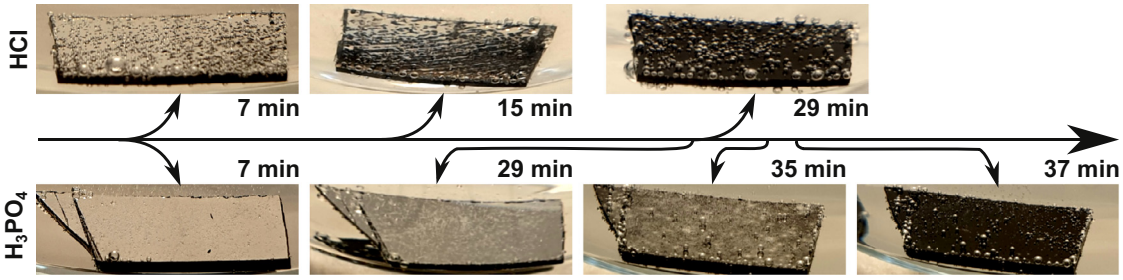

Fig. 7. Removal of a 200 nm film of Al on a Si substrate in HCl and H_3PO_4.

etching.

The limiting factors described above can be used to explain the development of Al gradient during its removal, which is shown in Fig. 3 (d–f). As the Al concentration in the as deposited sample is approximately 50%, it is clear from Fig. 3 that the etching rate in the first 2 h for etching in HCl and H_3PO_4 is faster than for the subsequent etching periods. This may be explained by a reduced etching rate due to the increased aspect ratio. The development of a gradient implies that the etching rate is different for different nanowires. In the case of HCl, this may be explained by the large dependence on defects in the protective Al_2O_3. In addition, variations in the NW quality such as diameter and level of verticality may limit diffusion in and out of the wire and provide different etching rates. These differences will also affect the NW removal by H_3PO_4, as the limitations of this process may be dominated by the transport of aluminum phosphate out of the pores. Therefore, the etching of Al NWs may be hindered locally, depending on the formation of aluminum phosphate. The process using H_3PO_4 results in a more curved concentration gradient of Al than compared to HCl, which may be explained by aluminum phosphate acting as a stronger barrier for some wires compared to Al_2O_3. Hence, although H_3PO_4 overall has a larger etching rate compared to HCl, etching of some wires may be hindered by a different mechanism compared to etching by HCl, thus not providing a linear gradient of Al.

We have shown in Fig. 3 and Fig. 5 that diluted H_2SO_4 is suitable, while concentrated H_2SO_4 only partially removes the Al NWs before the removal is stopped. This may be explained by the dehydrating properties of concentrated H_2SO_4. Water is required for the etching process to complex the formed Al^{3+} ions and as means of transporting these ions and the formed hydrogen gas from the reaction front, allowing access for new reactants. This is not an issue as long at the pore surface is sufficiently wetted, as this will force the H_2 bubble towards the surface. Due to dehydration from concentrated H_2SO_4, the surface becomes hydrophobic and the wetting properties are substantially reduced, which may trap H_2 within the pores and thus slows the etching process. A viable way to avoid such H_2 trapping is therefore to dilute the H_2SO_4 solution during etching.

5. Conclusion

We have studied selective etching of Al nanowires from nanostructured a-Si:Al using HCl, H_3PO_4, and H_2SO_4 as etchants, and their effect on surface oxidation, Al content, and porosity of the remaining porous a-Si. To estimate the Al gradient throughout the film during Al NW removal, we have used measurements of total reflectance in combination with theoretical modeling. H_3PO_4 is found to be the most efficient etching agent, but HCl provides a less oxidized a-Si in addition to a less reflecting film due to a more linear gradient of Al as a function of depth within the film. Due to its dehydrating properties, concentrated H_2SO_4 is not suitable as an etching agent as it stops the Al removal while a large fraction of Al NWs remains. Most Al may be removed given a sufficient etching time, resulting in a porous a-Si with oxidized surface with 25% porosity. We have shown that varying the etching agent may alter the optical and surface properties of the remaining porous a-Si film. It is therefore important to optimize the removal process depending on the application in mind, both with regard to choice of etching agent and etching time.

CRediT authorship contribution statement

T. Kjeldstad: Conceptualization, Methodology, Formal analysis, Investigation, Writing - original draft, Visualization. **A. Thøgersen:** Conceptualization, Resources, Writing - review & editing, Supervision, Funding acquisition. **M. Stange:** Investigation. **I.T. Jensen:** Investigation, Formal analysis. **O. Nilsen:** Methodology, Writing - review & editing. **A. Galeckas:** Validation, Writing - review & editing. **E. Monakhov:** Conceptualization, Resources, Writing - review & editing, Supervision.

Declaration of Competing Interest

The authors declare that they have no known competing financial interests or personal relationships that could have appeared to influence the work reported in this paper.

Acknowledgements

The Research Council of Norway is also acknowledged for the support to the Norwegian Micro- and Nano-Fabrication Facility, NorFab, [245963] and The Norwegian Transmission Electron Microscopy Centre, [197405].

References

[1] A.G. Cullis, L.T. Canham, P.D.J. Calcott, The structural and luminescence properties of porous silicon, J. Appl. Phys. 82 (1997) 909–965, https://doi.org/10.1063/1.366536.
[2] R. Bilyalov, L. Stalmans, J. Poortmans, Comparative analysis of chemically and electrochemically formed porous si antireflection coating for solar cells, J. Electrochem. Soc. 150 (2003) G216, https://doi.org/10.1149/1.1545468.
[3] J.H. Selj, A. Thøgersen, S.E. Foss, E.S. Marstein, Optimization of multilayer porous silicon antireflection coatings for silicon solar cells optimization of multilayer porous silicon antireflection coatings for silicon solar cells, J. Appl. Phys. 107 (2010) 074904, , https://doi.org/10.1063/1.3353843.
[4] M. Ge, J. Rong, X. Fang, C. Zhou, Porous doped silicon nanowires for lithium ion battery anode with long cycle life, Nano Lett. 12 (2012) 2318–2323, https://doi.org/10.1021/nl300206e.
[5] S. Bourderau, T. Brousse, D.M. Schleich, Amorphous silicon as a possible anode material for Li-ion batteries, J. Power Sources 81–82 (1999) 233–236, https://doi.org/10.1016/S0378-7753(99)00194-9.
[6] P. Granitzer, K. Rumpf, Porous silicon—a versatile host material, Materials (Basel) 3 (2010) 943–998, https://doi.org/10.3390/ma3020943.
[7] S. Thiyagu, H.-J. Syu, C.-C. Hsueh, C.-T. Liu, T.-C. Lin, C.-F. Lin, Optical trapping enhancement from high density silicon nanohole and nanowire arrays for efficient hybrid organic-inorganic solar cells, RSC Adv. 5 (2015) 13224–13233, https://doi.org/10.1039/C4RA13536A.
[8] K.-Q. Peng, X. Wang, L. Li, X.-L. Wu, S.-T. Lee, High-performance silicon nanohole solar cells, J. Am. Chem. Soc. 132 (2010) 6872–6873, https://doi.org/10.1021/ja910082y.
[9] A.M. Jani, D. Losic, N.H. Voelcker, Nanoporous anodic aluminium oxide: advances in surface engineering and emergin applications, Prog. Mater. Sci. 58 (2013) 636–704, https://doi.org/10.1016/j.pmatsci.2013.01.002.
[10] X. Xu, X. Fang, H. Zeng, T. Zhai, Y. Bando, D. Golberg, One-Dimensional nanostructures in porous anodic alumina membranes, Sci. Adv. Mater. 2 (2010) 273–294,

https://doi.org/10.1166/sam.2010.1094.
[11] W. Lee, S.-J. Park, Porous anodic aluminum oxide: anodization and templated synthesis of functional nanostructures, Chem. Rev. 114 (2014) 7487–7556, https://doi.org/10.1021/cr500002z.
[12] J. Sarkar, G. Gopal Khan, A. Basumallick, Nanowires: properties, applications and synthesis via porous anodic aluminium oxide template, Bull. Mater. Sci. 30 (2007) 271–290, https://doi.org/10.1007/s12034-007-0047-0.
[13] Y. Lin, X. Sun, M.S. Dresselhaus, Theoretical investigation of thermoelectric transport properties of cylindrical Bi nanowires, Phys. Rev. B 62 (2000) 4610–4623, https://doi.org/10.1103/PhysRevB.62.4610.
[14] Y. Wang, N. Herron, Nanometer-Sized semiconductor clusters: materials synthesis, J. Phys. Chem. 95 (1991) 525–532, https://doi.org/10.1021/j100155a009.
[15] E. Roduner, Size matters : why nanomaterials are different, Chem. Soc. Rev. 35 (2006) 583–592, https://doi.org/10.1039/b502142c.
[16] K. Fukutani, K. Tanji, T. Motoi, T. Den, Ultrahigh pore density nanoporous films produced by the phase separation of eutectic Al-Si for template-assisted growth of nanowire arrays, Adv. Mater. 16 (2004) 1456–1460, https://doi.org/10.1002/adma.200400268.
[17] K. Fukutani, Y. Ishida, T. Aiba, H. Miyata, T. Den, Characterization of nanoporous Si thin films obtained by Al–Si phase separation, Appl. Phys. Lett. 87 (2005) 253112, , https://doi.org/10.1063/1.2149292.
[18] A. Thøgersen, I.J.T. Jensen, M. Stange, T. Kjeldstad, D. Martinez-Martinez, O.M. Løvvik, A.G. Ulyashin, S. Diplas, Formation of nanoporous Si upon self-organized growth of Al and Si nanostructures, Nanotechnology 29 (2018) 315602, , https://doi.org/10.1088/1361-6528/aac36a.
[19] T. Kjeldstad, A. Thøgersen, M. Stange, A. Azarov, E. Monakhov, A. Galeckas, Monitoring selective etching of self- assembled nanostructured a-Si : Al fi lms, Nanotechnology 30 (2019) 135601, , https://doi.org/10.1088/1361-6528/aafb86.
[20] T. Kjeldstad, A. Thøgersen, M. Stange, I.T. Jensen, Surface effects and optical properties of self- assembled nanostructured a-Si : Al, Nanomaterials 9 (2019) 1106, https://doi.org/10.3390/nano9081106.
[21] F. Iacona, S. Lombardo, S.U. Campisano, F. Iacona, S. Lombardo, Characterization by x-ray photoelectron spectroscopy of the chemical structure of semi-insulating polycrystalline silicon thin films, J. Vac. Sci. Technol. B Microelectron. Nanom. Struct. Process. Meas. Phenom. 14 (1996) 2693, https://doi.org/10.1116/1.589006.
[22] A. Thøgersen, J.H. Selj, E.S. Marstein, Oxidation effects on graded porous silicon anti-reflection coatings, J. Electrochem. Soc. 159 (2012) 276–281, https://doi.org/10.1149/2.jes113659.
[23] F.J. Himpsel, F.R. McFeely, A. Taleb-Ibrahimi, J.A. Yarmoff, G. Hollinger, Microscopic structure of the SiO_2/Si interface, Phys. Rev. B 38 (1988) 6084.
[24] S. Iwata, A. Ishizaka, Electron spectroscopic analysis of the SiO_2 / Si system and correlation with metal – oxide – semiconductor device characteristics, J. Appl. Phys. 79 (1996) 6653, https://doi.org/10.1063/1.362676.
[25] M.J. Estes, G. Moddel, A model of size-dependent photoluminescence in amorphous silicon nanostructures : comparison with observations of porous silicon, Appl. Phys. Lett. 68 (1996) 1814–1816, https://doi.org/10.1063/1.116022.
[26] R.B. Wehrspohn, J.N. Chazalviel, F. Ozanam, I. Solomon, Spatial versus quantum confinement in porous amorphous silicon nanostructures, Eur. Phys. J. B 8 (1999) 179–193, https://doi.org/10.1007/s100510050681.
[27] O. Stenzel, Optical Coatings: Material Aspects in Theory and Practice, Springer, Berlin Heidelberg, 2014.
[28] H.A. MacLeod, Thin-Film Optical Filters, third ed., CRC Press, 2001.
[29] D.A.G. Bruggeman, Berechnung verschiedener physikalischer Konstanten von heterogenen Substanzen. I. Dielektrizitätskonstanten und Leitfähigkeiten der Mischkörper aus isotropen Substanzen, Ann. Phys. 416 (1935) 636–664, https://doi.org/10.1002/andp.19354160705.
[30] A. Thøgersen, M. Stange, I.J.T. Jensen, A. Røyset, A. Ulyashin, S. Diplas, Structure and optical properties of aSiAl and aSiAlHx magnetron sputtered thin films, APL Mater. 4 (2016) 036103, , https://doi.org/10.1063/1.4944506.
[31] H.R. Philipp, Optical properties of non-crystalline Si, SiO, SiOx and SiO_2, J. Phys. Chem. Solids. 32 (1971) 1935–1945, https://doi.org/10.1016/S0022-3697(71)80159-2.
[32] E.D. Palik, Handbook of optical constants of solids, Orlando, Academic Press, 1985.
[33] I.H. Malitson, Interspecimen comparison of the refractive index of fused silica, J. Opt. Soc. Am. 55 (1965) 1205–1209, https://doi.org/10.1364/JOSA.55.001205.
[34] M.W. Knight, N.S. King, L. Liu, H.O. Everitt, P. Nordlander, N.J. Halas, Aluminum for plasmonics, ASC Nano 8 (2014) 834–840, https://doi.org/10.1021/nn405495q.
[35] H.G. Tompkins, Spectroscopic Ellipsometry and Reflectometry : a User's Guide, first ed., Wiley, New York, 1999.
[36] P. Löbmann, Characterization of sol–gel thin films by ellipsometric porosimetry, J. Sol-Gel Sci. Technol. 84 (2017) 2–15, https://doi.org/10.1007/s10971-017-4473-1.
[37] D.A. Vermilyea, W. Vedder, Inhibition of the aluminum + water reaction, Trans. Faraday Soc. 66 (1970) 2644–2654, https://doi.org/10.1039/TF9706602644.